Low-Flow Limit in Slot Coating: Theory and Experiments

Marcio S. Carvalho
Imation Corporation, Oakdale, MN 55128

Haroon S. Kheshgi
Exxon Mobil Research and Engineering Co., Annandale, NJ 08801

The region of acceptable quality in the space of operating parameters of a coating process is called coating window. Their limits are set by coating defects. For the slot-coating process the low-flow limit is important. It corresponds to the maximum web speed at a given film thickness, or the minimum film thickness at a given web speed, at which the coating bead remains stable. The available viscocapillary model is based on the Landau-Levich equation, which is limited to small Capillary and Reynolds numbers. Under these conditions, the minimum film thickness that can be coated decreases with decreasing coating speed, but many coating processes do not occur at low Capillary numbers. It is important to determine the range of validity of the viscocapillary model and find the low-flow limit outside this range. The low-flow limit was determined here theoretically and experimentally. The 2-D Navier-Stokes equations with free surfaces describe liquid flow in the coating bead. Theoretical approaches solve the Navier-Stokes system by either using Galerkin's method with finite-element basis functions or applying a long-wave expansion. The minimum layer thickness at a set of parameters was determined by the turning point on the solution path as the thickness was diminished. The minimum film thickness was measured experimentally by determining the flow rate at which the coating bead breaks, leading to stripes of coated and uncoated web. Results show that the low-flow limit of the coating bead at large Capillary and Reynolds numbers fundamentally differs from that at their low numbers. At large Capillary and Reynolds numbers, the minimum film thickness that can be coated decreases with increasing coating speed. The coating window of the process is much larger than that in the literature, broadening the applicability of this coating method.

Introduction

Slot coating is used in the manufacturing processes of many different products. This method belongs to a class of coating methods known as *premetered coating*: the thickness of the coated liquid layer is set by the prescribed flow rate fed into the coating die and is independent of the process variables, making this class of method ideal for high-precision coating. However, the liquid flow in the application region (coating bead), and therefore the quality of the coated film, is strongly affected by operating parameters such as web speed, liquid properties, and the geometry of the die.

The region of acceptable coating quality in the space of the operating parameters of a coating process is usually referred to as the *coating window*. It is important to determine coating windows for the different coating methods in order to predict whether a given method can be used to coat a product at a prescribed production rate. Coating windows can be constructed either from extensive experimentation or from theoretical modeling of the coating flow. The experimental approach is generally expensive. In contrast, with a reliable theoretical model, many aspects of coating quality can be com-

Correspondence concerning this article should be addressed to M. S. Carvalho.
Current address of M. S. Carvalho: Dept. of Mechanical Engineering, Pontifícia Universidade Católica do Rio de Janeiro (PUC-Rio), Rua Marquês de São Vicente 225, Gávea, Rio de Janeiro, RJ, 22453-900, Brazil.

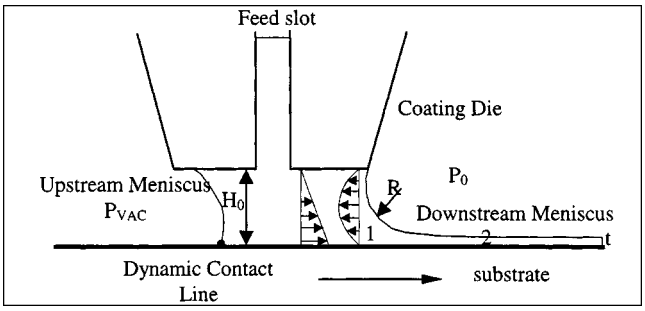

Figure 1. Coating bead of a slot coater.

puted over large ranges of variables at relatively low cost. Because theoretical models are rarely complete, however, theoretical predictions should be compared with experiments in order to validate them.

Figure 1 shows a two-dimensional cross section of a slot-coating bead. The coating liquid is pumped through the feed slot and bridges between the coating die and the solid substrate, the web, forming the coating bead. The coating bead is bounded by two gas–liquid interfaces. It is clear that physics sets the operating parameters at which this two-dimensional free surface flow exists. In order to sustain the coating bead at higher speeds, vacuum is usually applied to the gas upstream from the upstream meniscus (Beguin, 1954).

Higgins and Scriven (1980) extended the work of Ruschak (1976) and analyzed the operating parameters at which capillary and viscous forces could be balanced over a two-dimensional cross section of the coating bead of a slot coater. The results of their viscocapillary model led to a feasibility window in the plane of vacuum pressure and web speed. Since then, several experimental and theoretical analyses that determine the vacuum limits for stable operation have been reported in the literature (Sartor, 1990; Gates, 1996). However, vacuum pressure is usually not a limitation in slot coating of thin films. In the coating windows presented in the literature, there is always a range of vacuum at which the coating bead is stable at Capillary numbers below a critical value.

A more important limit, from a practical point of view, is what is generally referred to as the *low-flow* limit. This limit corresponds to the maximum web speed possible at a given film thickness, or the minimum film thickness at a given web speed, at which the flow is stable. The low-flow limit of slot coating has been studied by Lee and Liu (1992); however, their experiments were performed without any vacuum pressure applied to the upstream meniscus, and therefore their results do not represent the actual low-flow limit of industrial situations.

The basic mechanism that defines the low-flow limit can be well described by the viscocapillary model. The main flow under the die land is a combination of a Couette and a Poiseuille contribution, as shown in Figure 1. At a given coating gap, H_0, and constant speed, V, the flow rate associated with the Couette contribution is constant. As the film thickness t (and therefore the flow rate) decreases, the Poiseuille contribution (and therefore the adverse pressure gradient in the downstream meniscus region) has to increase. The minimum flow rate possible (minimum film thickness) is determined by the maximum pressure gradient possible at the downstream meniscus. The pressure gradient can be estimated by analyzing the pressure difference between points 1 and 2 (see Figure 1). It is approximately determined by the radius of curvature of the liquid/gas interface, R, and the surface tension of the liquid, σ:

$$p_2 - p_1 = p_0 - p_1 = \frac{\sigma}{R}.$$

The maximum pressure gradient occurs at the smallest radius of curvature possible. If the shape of the free surface is assumed to be cylindrical, the smallest radius that can be fit between the die and the web is given by

$$R = \frac{H_0 - t}{2}.$$

Ruschak (1976) extended the work of Landau and Levich (1942) and showed that the pressure drop across the downstream meniscus can be related to the film thickness, web speed, and liquid properties:

$$p_0 - p_1 = 1.34\,Ca^{2/3}\frac{\sigma}{t}.$$

The capillary number is defined as $Ca \equiv \mu V/\sigma$, and it indicates the ratio between viscous (μ is the viscosity of the liquid) to surface tension forces. The operating parameters that set the low-flow limit can be determined by combining the three previous equations:

$$Ca = \frac{\mu V}{\sigma} = 0.65\left(\frac{2}{(H_0/t) - 1}\right)^{3/2}. \qquad (1)$$

This relation is plotted in Figure 2. Above the solid line, the coating bead is unstable and the two-dimensional steady flow does not exist. In experiments, crossing the low-flow limit from stable to unstable, the uniform coated layer gives way to alternating uncoated and coated stripes. This defect is generally referred to as *rivulets*. It is clear from the plot that, at a

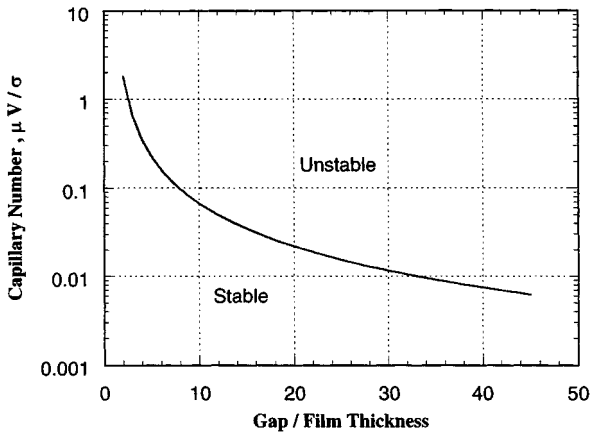

Figure 2. Low-flow limit predicted using the viscocapillary model.

fixed coating gap, the minimum possible film thickness increases the Capillary number increases, that is, higher production speeds require thicker wet layers.

Because the viscocapillary model was derived from the Landau-Levich equation, it is only valid at low Capillary numbers, that is, typically low speed and/or low viscosity. However, many coating processes do not operate at low capillary numbers. Experiments by Sartor (1990) have shown examples where the viscocapillary model fails to predict the correct maximum coating speed. It is important to establish what is the range of validity of the viscocapillary model, and moreover to find the low-flow limit outside this range.

The viscocapillary model indicates that slot coating is better suited for low-viscosity liquids. The limitation on web speeds for higher-viscosity liquids can be illustrated by the following example: Suppose a liquid film of thickness $t = 0.6$ mil (≈ 15 μm) is to be coated onto a substrate by the slot-coating method with a coating gap of $H_0 = 4$ mil (≈ 100 μm). The solution has viscosity of $\mu = 20$ cP and surface tension of $\sigma = 25$ dyn/cm. The maximum possible line speed predicted by the viscocapillary model is approximately equal to $V = 30$ ft/min (≈ 0.15 m/s). Such low speeds may not satisfy the economic requirements of some products.

In this work, the low-flow limit at different operating conditions, including high Capillary and Reynolds numbers, was determined by both theory and experiments. First, the low-flow limit was estimated by the film-profile equation derived from a long-wave expansion to the Navier-Stokes equation, as described by Kheshgi (1989). The predictions were compared with the complete theoretical approach that consisted of solving the two-dimensional Navier-Stokes equations with free surfaces that describe liquid flow in the coating bead by the Galerkin/finite-element method. At each operating condition (liquid properties, coating gap, and web speed), first-order, pseudo-arc-length continuation was used to construct a solution path as the flow rate fed into the die was diminished. The minimum film thickness corresponded to the flow rate at which a turning point on the solution path occurred. The experimental procedure followed a path similar to the theoretical calculations. A coating bead was established at each condition. Then, the flow rate into the die was slowly decreased until the coated layer broke into stripes of coated and uncoated web. The experiments were done using liquids with different viscosity in order to cover a wide range of Capillary numbers.

Film-Profile Equation Model

By application of a long-wave expansion to the Navier-Stokes system for film flows, Kheshgi (1989) derived an approximate film-profile equation (FPE) for the evolution of finite-amplitude disturbances to Newtonian liquid films. FPEs based on a long-wave expansion are asymptotically accurate for films where the disturbance is long relative to the film thickness, and the Reynolds number is low. FPEs are an extension of the viscocapillary model discussed in the Introduction, and include higher-order terms. Moreover, one form of FPE was found to represent well the shape of the film downstream from a slot coater at moderate Reynolds and Capillary numbers. Note that film thickness decreases more rapidly with distance from the slot in flows with higher Capillary number. In this section we apply this FPE to estimate the low-flow limit in slot coating, and in the following section on the two-dimensional model, we compare the results to finite-element solutions of the Navier-Stokes system.

The form of FPE given by Kheshgi (1989) adapted to steady films translating in the x-direction is

$$\frac{d(2H)}{dX} = 3Ca\left(\frac{1}{Y^3} - \frac{1}{Y^2}\right) + \frac{6}{35}N_{Re}Ca\frac{dY}{dX}\left(\frac{1}{Y} + \frac{1}{Y^2} - \frac{9}{Y^3}\right). \quad (2)$$

The position of the free surface in Cartesian coordinates (X, Y) is made dimensionless with the length scale, t, the final film thickness. The full representation of the curvature of the free surface is $2H$, which in Cartesian coordinates is given by

$$2H = \frac{d^2Y}{dX^2}\Bigg/\left[1 + \left(\frac{dY}{dX}\right)^2\right]^{1/2}. \quad (3)$$

The Reynolds number based on the deposited film thickness, t, is $N_{Re} \equiv \rho Vt/\mu$.

The shape of the downstream free surface in a slot coater, that is, the solution of the FPE, is obtained by numerical integration of Eq. 2. It was represented by a system of first-order ODEs in arc-length coordinates, as was done by Kheshgi et al. (1992) to estimate film profiles in dip coating. The integration begins far downstream from the slot, starting with the initial conditions:

$$Y = 1 + \epsilon, \qquad \frac{dY}{dX} \cong \theta = -\epsilon\lambda, \quad \text{and} \quad \frac{d^2Y}{dX^2} \cong 2H = \epsilon\lambda^2,$$

where λ is the exponential decay rate of the film to its final film thickness $Y = 1$, determined by the solution of the linearized version of Eq. 2, and ϵ is a small specified coefficient (such as 0.01). The inclination of the film is represented by the angle θ. If N_{Re} and Ca are small, the region of the free surface that is highly inclined would be much thicker than the final film thickness, viscous and inertial forces would be small, and the film curvature would be approximately constant, that is, the righthand side of Eq. 2 would be small. Integration is continued in arc-length coordinates until a maximum value of the coordinate Y is reached. In all cases this corresponded to $\theta = \pi$, with a film profile that has turned upside-down. Figure 3 shows the computed downstream meniscus at $Re = 0$ and different Capillary numbers. As the Capillary number falls, $Y_{\max}$ increases. The low-flow limit at each operating condition can be estimated based on the values of $Y_{\max}$, as explained in the following subsection.

Use of film-profile equation to estimate the low-flow limit in slot coating

As is shown in Figure 3, at each Capillary number, Reynolds number, and final film thickness, t, there is a maximum value for the dimensionless coordinate Y at the point where $\theta = \pi$. The low-flow limit can be estimated by assuming that $Y_{\max}$

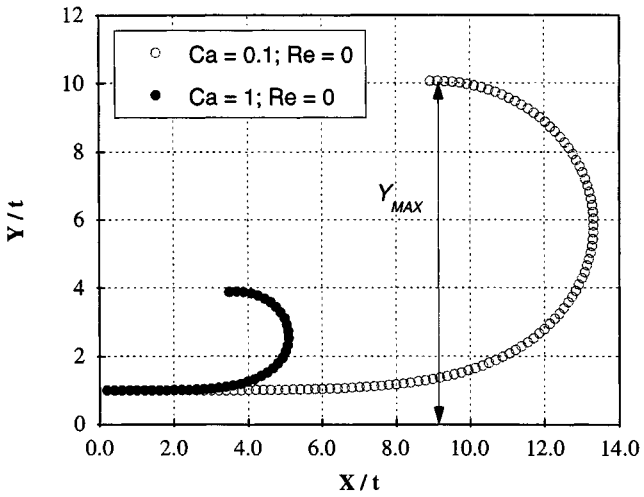

Figure 3. Downstream meniscus predicted by the FPE at *Ca* = 0.1 and *Ca* = 1 and vanishing Reynolds number.

represents the ratio G between the maximum slot gap possible H_0 and the final film thickness t at a given set of conditions, that is, $Y_{\max} = G = H_0/t$. A stability map, similar to the one presented in Figure 2, but now including the effect of Reynolds number and higher-order terms, can be constructed with the predictions of the FPE. Note that the value of $G = H_0/t$ calculated in the way described in this section is a function of Ca and N_{Re}, which are specified. To estimate G as a function of Ca and $Re \equiv \rho V H_0/\mu$, N_{Re} is adjusted iteratively to yield a specified $Re = N_{Re}G(Ca, N_{Re})$.

The low-flow-limit map predicted by the FPE is shown in Figure 4, together with the viscocapillary model results. In order to relate the effect of the web speed to only one dimensionless parameter, such as capillary number, the results are plotted in terms of the Property number, defined as the

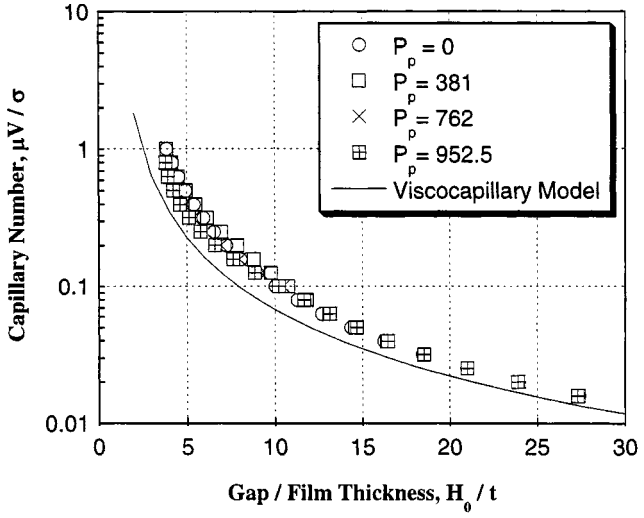

Figure 4. Low-flow limit predicted using the FPE at different Property numbers.

ratio of Reynolds to Capillary number, or $P_p \equiv Re/Ca = \rho\sigma H_0/\mu^2$, and therefore independent of web speed. At low Capillary number, $Ca < 0.01$, the predicted critical gap to film thickness at the onset of the low-flow limit is virtually the same as the one predicted by the viscocapillary model. The effect of inertia, represented in terms of Property number, is negligible at this range. At higher Capillary numbers, for example, $Ca > 0.01$, the FPE predicts a gap-to-film-thickness ratio larger than the one obtained with the viscocapillary model. The results obtained with the FPE show the small effect of inertia on the onset of the low-flow limit. At large Capillary numbers, as the Property number rises, the critical gap-to-film-thickness ratio initially increases, reaches a maximum, and then decreases. The approximation used to derive the FPE is, however, valid only at low Capillary and Reynolds numbers.

Two-Dimensional Model

In order to verify the predictions of the FPE, and to extend the analysis to even higher Capillary and Property numbers, where the long-wave expansion is not valid, the flow in the coating bead was described by the complete two-dimensional, steady-state Navier-Stokes system. This section describes the formulation, solution method, and predictions obtained with this more complete description of the flow.

Governing equations and boundary conditions

The Navier-Stokes system for viscous free-surface flows is described in detail by Kizstler and Scriven (1983). The particular case of the flow on a slot-coater bead was first presented by Sartor (1990). This section recapitulates the governing equations and lays out the boundary conditions used.

Figure 5 shows the domain used in this analysis. The velocity and pressure fields are governed by the momentum and continuity equations, which in dimensionless form are

$$Re\,\boldsymbol{v}\cdot\nabla\boldsymbol{v} - \nabla\cdot\boldsymbol{\sigma} = 0, \qquad \nabla\cdot\boldsymbol{v} = 0. \tag{4}$$

For a Newtonian liquid, the total stress is $\sigma = -pI + \nabla\boldsymbol{v} + (\nabla\boldsymbol{v})^T$. The Reynolds number $Re = \rho V H_0/\mu$ measures the ratio of inertia to viscous forces. The web velocity is represented by V, and H_0 is the gap, that is, the distance between the coating die and the substrate. The dimensionless geometric parameters are the gap-to-film-thickness ratio $G = H_0/t$, and the dimensionless slot height $S = H_s/H_0$.

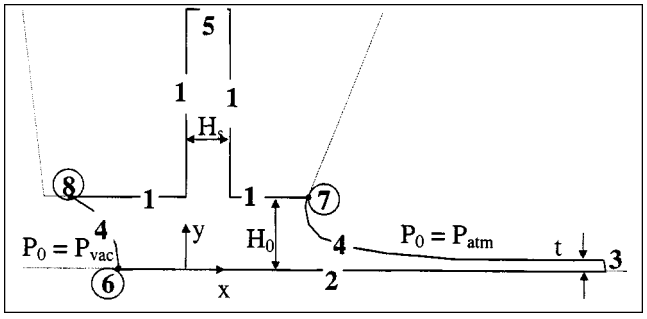

Figure 5. Flow domain with boundary conditions.

The no-slip and no-penetration conditions applies at the die walls and at the substrate:

$$\boldsymbol{v} = 0, \qquad \text{at the die walls } (\mathbf{1}) \tag{5}$$

$$\boldsymbol{v} = Vi, \qquad \text{at the substrate } (\mathbf{2}) \tag{6}$$

Here, V is the web speed. At the outflow plane (**3**), the directional derivative of velocity is set to zero:

$$n \cdot \nabla \boldsymbol{v} = \mathbf{0}. \tag{7}$$

At the free surfaces (**4**), the traction in the liquid balances the capillary pressure, and there is no mass flow across the gas–liquid interface:

$$n \cdot \sigma = \frac{1}{Ca}\frac{dt}{ds} - nP_0, \qquad n \cdot \boldsymbol{v} = 0, \tag{8}$$

where t is the unit vector tangent to the interface and P_0 is the pressure of the air. At the downstream free surface, the air pressure is usually atmospheric, that is, $P_0 = P_{\mathrm{ATM}}$. At the upstream gas–liquid interface, vacuum is usually applied in order to stabilize the coating bead, that is, $P_0 = P_{VAC}$. The dimensionless vacuum pressure is defined as $Vac = P_{VAC}H_0/\sigma$. The Capillary number $Ca = \mu V/\sigma$ measures the ratio between viscous and capillary forces (σ is the liquid surface tension).

At the inflow plane (**5**), that is, at the die feeding slot, the flow is assumed to be fully developed:

$$i \cdot \boldsymbol{v} = 0; \qquad j \cdot \boldsymbol{v} = -\frac{6Q}{H_s}\left[\left(\frac{x}{H_s}\right) - \left(\frac{x}{H_s}\right)^2\right], \tag{9}$$

where Q is the flow rate fed into the coating die. It defines the thickness t of the liquid layer deposited onto the substrate: $t = Q/V$.

At the dynamic contact line (**6**), the Navier slip condition was used instead of the no-slip condition and a dynamic contact angle $\theta_d = 110^0$ was imposed:

$$\frac{1}{\beta} t_w \cdot (\boldsymbol{v} - Vi) = t_w \cdot (n_w - \sigma); \qquad n_w \cdot n_{fs} = \cos(\theta_d), \tag{10}$$

where β is the slip coefficient, t_w and n_w are the unit tangent and normal vector to the wall, and n_{fs} is the unit vector normal to the free surface. For a better description of the flow in this region, a contact angle as a function of Capillary number would be more appropriate. However, because the low flow limit is set by a force balance at the downstream free surface, and it is virtually insensitive to the flow close to the dynamic contact line, the dynamic contact angle was assumed to be constant for the sake of simplicity.

The static contact line attached to the downstream free surface (**7**) is pinned at the sharp edge of the die, that is, the position x_{sd} of the downstream static contact line is fixed:

$$x_{sd} = X_{edge}. \tag{11}$$

The upstream static contact line (**8**) is free to move along the die face, that is, the y-coordinate of the upstream static contact line is fixed. In this case, the static contact angle θ_s of the free surface with the die face has to be specified:

$$j \cdot x_{su} = H_0; \qquad n_w - n_{fs} = \cos(\theta_s). \tag{12}$$

Solution method

Because of the free surfaces, the flow domain at each parameter is unknown *a priori*. In order to solve this free-boundary problem by means of standard techniques for boundary-value problems, the set of differential equations and boundary conditions posed in the unknown domain (Eqs. 4–12) has to be transformed to an equivalent set defined in a known reference domain. This transformation is made by a mapping $x = x(\xi)$ that connects the two domains. The mapping used here is the one presented by de Santos (1991). He showed that a functional of weighted smoothness can be used successfully to construct the sorts of maps involved here. The inverse of the mapping that minimizes the functional is governed by a pair of elliptic differential equations identical with those encountered in diffusional transport with variable diffusion coefficients. The coordinates ξ and η of the reference domain satisfy

$$\nabla \cdot (D_\xi \nabla \xi) = 0; \qquad \nabla \cdot (D_\eta \nabla \eta) = 0, \tag{13}$$

where D_ξ and D_η are diffusion-like coefficients used to control element spacing. Boundary conditions are needed in order to solve the second-order partial differential equations (Eq. 13). Along solid walls and synthetic inlet and outlet planes, the boundary is located by imposing a relation between coordinates x and y from the equation that describes the shape of the boundary, and stretching functions are used to distribute the points along the boundaries. The free boundaries (gas–liquid interfaces) are located by imposing the kinematic condition (Eq. 8b). The discrete version of the mapping equations is generally referred to as mesh-generation equations.

The Navier-Stokes system and the mapping (mesh-generation) equations were solved all together by the Galerkin/finite-element method. Biquadratic basis functions were used to represent both the velocity and the mapping from the reference to the physical domain. The basis functions used to represent the pressure field were piecewise, linear, and discontinuous. Details of the weak formulation of this class of problems can be found elsewhere (Kistler and Scriven, 1983).

Once all the variables are represented in terms of the basis functions, the system of partial differential equations reduces to simultaneous algebraic equations for the coefficients of the basis functions of all the fields. This set of equations is nonlinear and sparse. It was solved by Newton's method. The linear system of equations at each Newtonian iteration was solved using a frontal solver.

Newton's method converges quadratically close to the solution. However, it can fail to converge if the initial guess is not close enough to the solution or if the solution does not exist for a given set of parameters. In order to improve the likelihood of convergence and to obtain solutions around turning

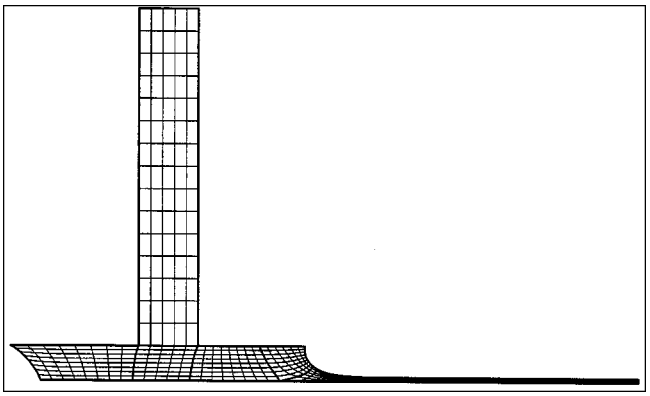

Figure 6. Representative mesh used to discretize the problem: 411 elements and 8,373 unknowns.

points, a pseudo-arc-length continuation method, as described by Keller (1977), was used. Solutions were not calculated exactly at the turning point, where Newton's method would not converge. The turning point was considered to be the last solution computed before the derivative of the changing parameter with respect to the solution norm switches sign.

The domain was divided into 411 elements, with 8373 unknowns. A representative mesh is shown in Figure 6.

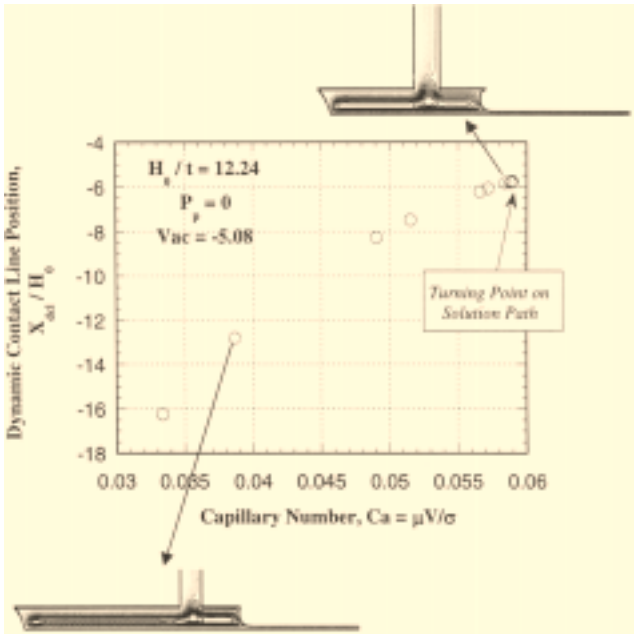

Figure 7. Path of flow states at fixed film thickness.

The states are characterized by the position of the dynamic contact line. Inserts represent streamlines of selected flow states.

Results

In order to relate the effect of the web speed solely to one of the dimensionless parameters (Capillary number), it is useful to define the Property number $P_p \equiv Re/Ca = \rho\sigma H_0/\mu^2$, that is, a function of the liquid properties and the coating gap, and invariant to substrate speed.

The operating conditions at the low-flow limit were determined by two different approaches. In the first, the coated-layer thickness was fixed and the web speed increased until a turning point on the solution path was encountered. The critical Capillary number at the chosen gap-to-thickness ratio was calculated from the value of the web velocity at the turning point. The second approach consisted of following the solution path at a fixed web speed. The flow rate, and therefore the film thickness, was decreased until a turning point was encountered. The critical gap-to-thickness ratio was calculated from the value of the flow rate at the turning point. The theoretical predictions show that the two approaches are equivalent and lead to the same critical pair of Capillary number and gap-to-thickness ratio.

Figure 7 shows a path of solutions computed at $H_s/H_0 = 1.75$, $H_0/t = 12.24$, $P_p = 0$ (no inertia), and $Vac = -5.08$. The flow states are characterized by the position of the dynamic contact line. It is pulled closer to the feeding slot as the web speed rises. A turning point occurs at $Ca = 0.0589$. Above that speed, a two-dimensional, steady-state solution could not be found. In practice this would signal the low-flow limit. Because of the high gap-to-thickness ratio, a large recirculation is present at all Capillary numbers. As the Capillary number increases, the downstream meniscus becomes more curved (smaller radius of curvature) in order to increase the adverse pressure gradient under the free surface. Figure 8 details the shape of the downstream free surface. At the turning point, that is, $Ca = 0.0589$, the angle between the gas–liquid interface and the die face is very close to zero. The hypothesis that the static contact line is pinned at the sharp edge of the die is probably not valid at such conditions. In practice, if the web speed is raised above the critical value, the meniscus would recede and the coating bead would break.

Figure 9 shows the solution path obtained at a Capillary number of $Ca = 0.33$, $H_s/H_0 = 1.75$, $P_p = 0$, and $Vac = -13.5$. The plot shows how the position of the dynamic contact line varies with the flow rate fed into the die, that is, the film thickness deposited on the substrate. As the coated film be-

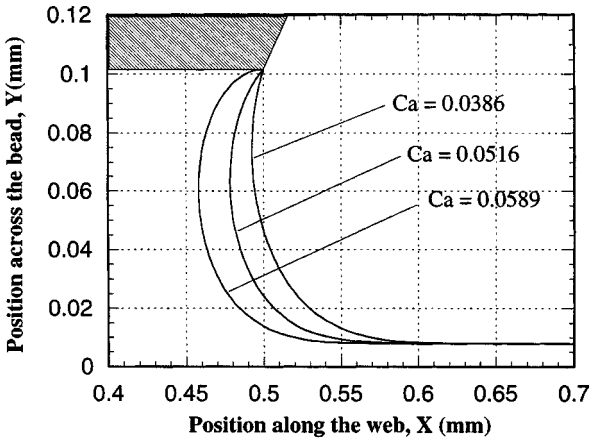

Figure 8. Downstream free surface shape as a function of Capillary number.

$H_0/t = 12.24$ and $P_p = 0$.

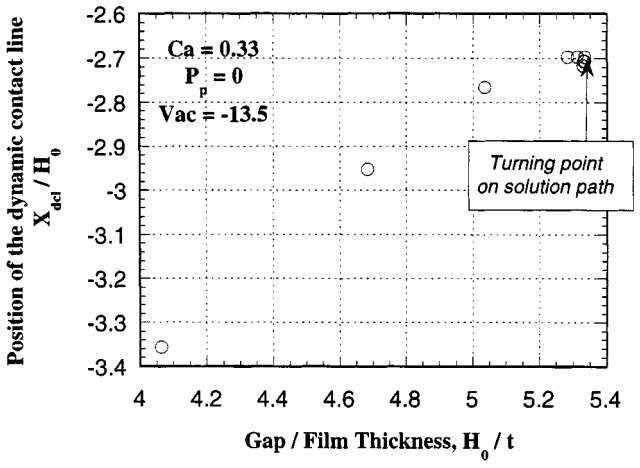

Figure 9. Path of flow states *Ca* = 0.33.

The states are characterized by the position of the dynamic contact line.

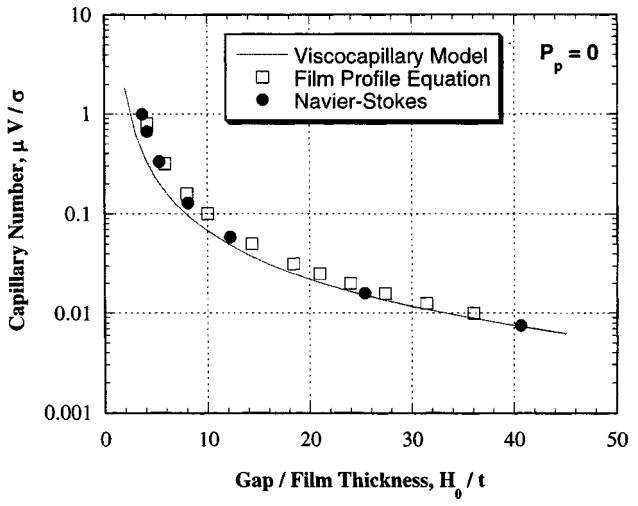

Figure 11. Low-flow-limit predictions by: viscocapillary model, FPE, and Navier-Stokes equations.

Inertial effects were neglected, that is, $P_p = 0$.

comes thinner, the dynamic contact line is pulled toward the die feeding slot. A two-dimensional, steady-state solution could not be found at a gap-to-thickness ratio above $H_0/t =$ 5.33. Again, the turning point marked the low-flow limit at this particular Capillary number. The shapes of the downstream free surfaces at a gap-to-thickness ratio equal to 4.06, 5.03, and 5.33 are shown in Figure 10. The behavior is the same one observed as the Capillary number was increased. As the gap-to-thickness ratio rises, that is, smaller film thickness, the meniscus becomes more curved. At the turning point, the angle between the free surface and the die face is almost zero.

Solution paths similar to those presented in Figures 7 and 9 were constructed at different ratios between gap and film thickness and Capillary numbers. The slot height was kept constant and equal to $H_s/H_0 = 1.75$. The parameters at which the turning point occurs in each solution path are mapped in Figure 11. They correspond to the low-flow limit at $P_p = 0$. The plot also shows the critical conditions predicted by the viscocapillary model and FPE. As expected, both the FPE and viscocapillary model are very accurate at low Capillary numbers ($Ca < 0.01$). At these conditions, the predictions of the full Navier-Stokes equation, FPE, and viscocapillary model are virtually the same. At higher Capillary numbers, the viscocapillary model underpredicts the critical gap to film thickness (overpredicts the critical film thickness) when compared with the other two approaches. The discrepancy increases with Capillary number. The relative difference is around 10% at $Ca \approx 0.1$ and as high as 30% at $Ca \approx 1$. The FPE results are close to the Navier-Stokes predictions over the entire range of Capillary number; the largest relative difference was below 10%.

The low-flow limit predictions presented up to this point were obtained by neglecting inertial effects, that is, $P_p = 0$ ($Re = Ca \cdot P_p$). The critical parameters at which the turning points occur on the solution path, when inertial effects are considered, are illustrated in Figure 12. Again, the solid line

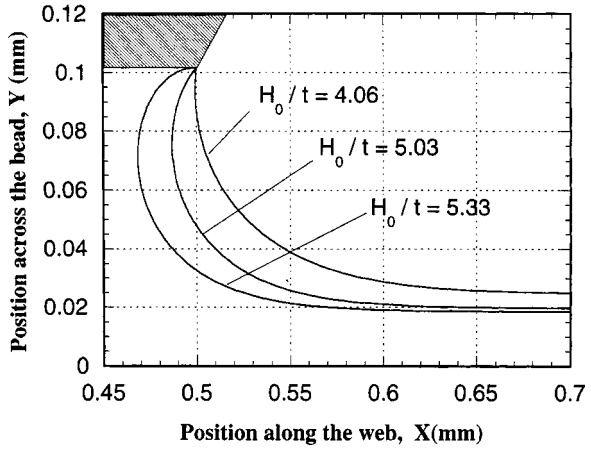

Figure 10. Downstream free surface shape at different gap-to-thickness ratio: *Ca* = 0.33.

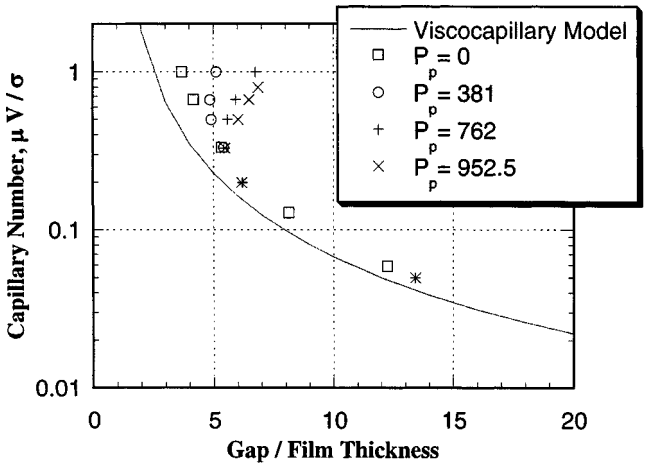

Figure 12. Inertial effects on the low-flow limit.

represents the viscocapillary model predictions. At low Capillary numbers, the low-flow limit is virtually insensitive to the Property number, that is, inertial effects are not important in the parameter range explored in this analysis. At larger Capillary numbers ($Ca > 0.3$ for the cases analyzed here), the critical gap-to-thickness ratio is strongly dependent on the Property number. Inertial effects delay the onset of the low-flow limit to thinner film thickness. The results are different from those predicted by the FPE. Although the simplified model is accurate when inertial effects are neglected, it cannot describe well the flow at finite Reynolds number. An interesting phenomenon occurs when inertial effects become significant. Above a certain coating speed (that is, Capillary number at a fixed Property number), the relationship between the critical Capillary number and critical gap-to-thickness ratio changes. At low Capillary numbers, the minimum possible film thickness that can be coated increases with web speed. At high Capillary numbers, the critical ratio of gap to film thickness that sets the low-flow limit increases with Capillary number; the minimum possible film thickness that can be coated decreases as web speed rises. The actual coating window for slot coating is larger than the one presented in the literature.

The practical consequence of this behavior is very important: thinner films can be achieved by raising the coating line speed. At a fixed coating gap and film thickness, there are two ranges of Capillary number at which the coating bead exists, $Ca < Ca_1^*$ and $Ca > Ca_2^*$. The first limit Ca_1^* is the one presented before in the literature and that can be fairly well predicted by the simple viscocapillary model. This limit is the low Capillary number limit. The second limit Ca_2^* is the limit found when inertial effects were incorporated into the theoretical model. This limit is the high Capillary number limit. As is clear from Figure 12, the transition from one regime to the other is a function of Property and Capillary numbers. At $P_p = 381$, the transition occurs at $Ca \cong 0.7$, while at $P_p = 952.5$, it happens at $Ca \cong 0.3$. Actually, the two different regimes are defined by the intensity of inertial forces, and they could be referred to as the *low inertia regime* and the *high inertia regime*.

The importance of this extended coating window is better quantified by the example discussed before: Suppose a solution of $\mu = 20$ cP, $\sigma = 25$ dyn/cm is to be coated at a thickness of $t = 0.6$ mil (≈ 15 μm) with a coating gap of $H_0 = 4$ mil ($H_0/t = 6.67$). The maximum possible line speed predicted by the viscocapillary model or by the low Capillary number limit of the Navier-Stokes solution is approximately equal to $V_{max} = 30$ ft/min (≈ 0.15 m/s). Using the high Capillary number limit, the process could be carried out with a web speed of $V > 250$ ft/min (≈ 1.25 m/s).

The extended coating window is bounded by another coating defect at even higher Capillary numbers. Above a certain value, instabilities at the dynamic contact line lead to a nonperfect wetting of the liquid onto the substrate. The defect is generally referred to as *air entrainment*. This limit was not analyzed in this work. When coating very thin films, the coating becomes unstable at Capillary numbers lower than the critical values associated with air entrainment.

As discussed before, the low-flow limit occurs when the downstream meniscus recedes into the coating bead in order to decrease the radius of curvature of the free surface. When inertia becomes significant, the momentum of the liquid tends to counteract this receding action. Figure 13 illustrates this behavior by showing how the free-surface shape changes as the line speed is raised, at Property number $P_p = 762$ and gap-to-thickness ratio $H_0/t = 5.08$. At these conditions, the coating bead exists at all Capillary numbers explored, and a turning point on the solution path was not found up to $Ca = 1.006$. The length necessary for the coated film to achieve its final thickness is much longer than that obtained when inertial effects are not taken into account (compare Figures 8 and 10). First, as the web speed is raised, and consequently as the Capillary number increases, the radius of curvature of the downstream free surface decreases and so does the angle between the meniscus and the die face at the static contact line. At higher Capillary numbers, an opposite effect occurs: as the web speed increases, inertial forces push the meniscus away from the coating bead, increasing the radius of curvature of the downstream meniscus and the angle between the free surface and the die face. The free surface becomes more stable (further away from the low-flow limit in the parameter space) as the line speed is raised.

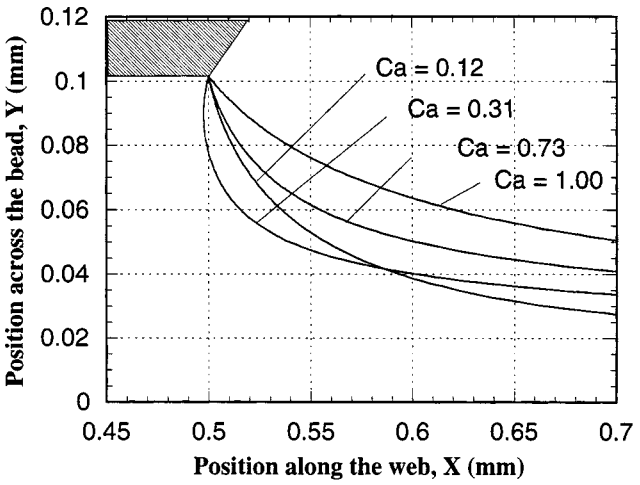

Figure 13. Downstream free surface shape at different Capillary numbers: $P_p = 762$.

The FPE model could not capture this behavior because it only describes the flow close to the downstream meniscus, not taking into account the effect of the flow in the coating bead. Figure 14 compares the downstream free surface predicted by the Navier-Stokes and the FPE. The FPE results were accurate far away from the slot die for all values of P_p and Ca. Close to the die, the results deteriorate as the Property number increases.

Because vacuum pressure is always used in slot coating operation, its effect on the onset of the low-flow limit was also analyzed. Figure 15 shows two sets of solutions at $H_0/t = 10.16$, $P_p = 952.5$, and vacuum pressures of $P_{VAC}H_0/\sigma = -4.23$ and -8.46. The higher vacuum pulls the upstream free surface away from the feeding slot, making the bead longer. However, the turning point on both sets of solutions that characterizes the low-flow limit occurs at the same Capillary number ($Ca = 0.081$). It is important to notice that this condition corresponds to the low inertia/capillary regime. At the high inertia/capillary regime, the behavior is completely dif-

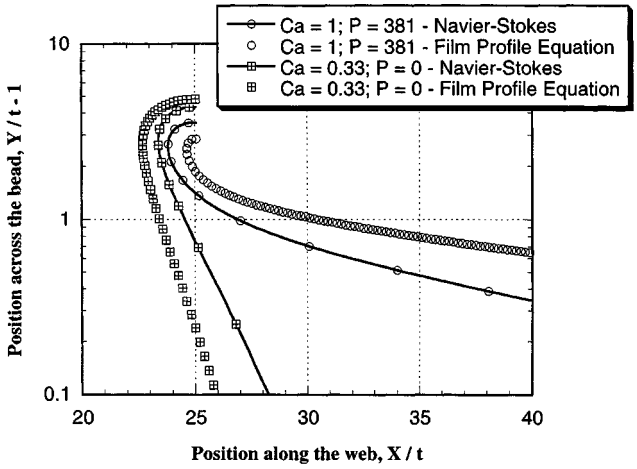

Figure 14. Comparison of downstream free surface predicted by FPE and Navier-Stokes equation.

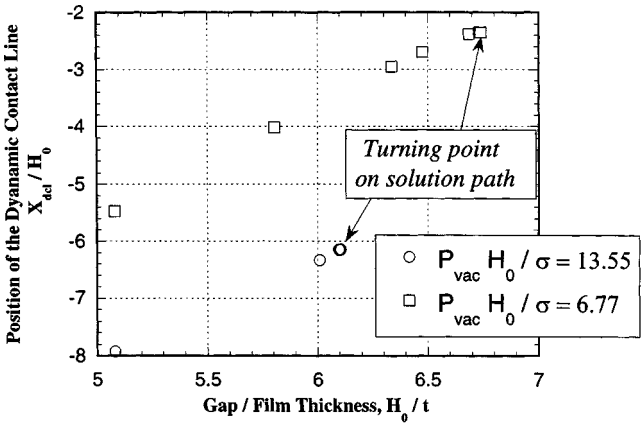

Figure 16. Solution path at $Ca = 1$ and $P_p = 762$ and different vacuum pressures.

Flow states are characterized by the position of the dynamic contact line.

ferent. Figure 16 illustrates two solution paths at $Ca = 1$, $P_p = 762$, and $P_{VAC}H_0/\sigma = -6.77$ and -13.55. The turning point that characterizes the low-flow limit occurs at different conditions. As the coating bead got longer (higher vacuum pressure), the onset of the low-flow limit occurred at smaller gap-to-film thickness ratio. The explanation for this dependence is discussed next.

It is clear from the analysis presented in this section that there are two distinct mechanisms for the onset of the low-flow limit: a *low inertia/Capillary* and a *high inertia/Capillary* regime.

The first regime has been extensively discussed in the literature and is well described by a simple viscocapillary model. The onset of the low-flow limit is dictated by the balance of viscous and surface-tension forces, and the critical pair of Capillary number (web speed) and gap-to-film-thickness ratio can be estimated by Eq. 1, or obtained with a higher degree of accuracy with the FPE model. When inertial forces become important, the shape of the downstream free surface is strongly affected by the momentum of the liquid in the coating bead. The onset of the low-flow limit is not governed by the balance between viscous and surface-tension forces alone. The relationship between the critical gap-to-film thickness and the web speed at the onset of the low flow limit can be explained by boundary-layer theory. At high Reynolds number, the thickness of the film that the web can accelerate depends on the growth of a viscous boundary layer. When the web speed is high, the viscous boundary layer grows slowly, and the length necessary for it to grow to the final film thickness t is large, as shown in Figure 17. This can be illustrated by the shape of the downstream free surfaces shown in Figure 13. As the web speed falls, the growth length L_b decreases according to

$$L_b = k\frac{\rho V t^2}{\mu}. \tag{14}$$

From Figure 17, it is clear that there is a critical growth length below which a two-dimensional coating bead cannot exist. This critical growth length L_b^*, which is directly related to the length of the coating bead, defines the critical web

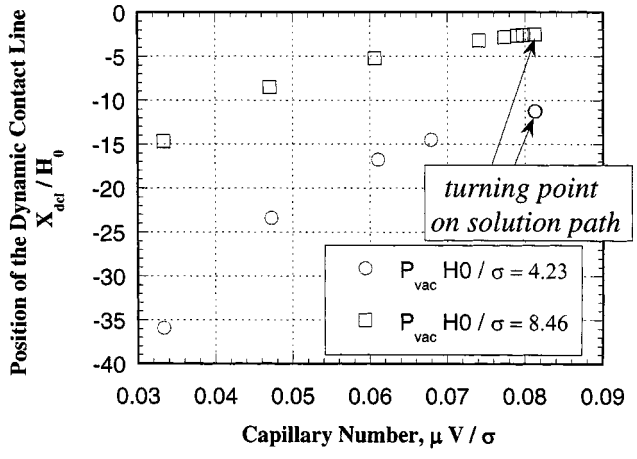

Figure 15. Solution path at $H_0/t = 10.16$ and $P_p = 952.5$ and different vacuum pressures.

Flow states are characterized by the position of the dynamic contact line.

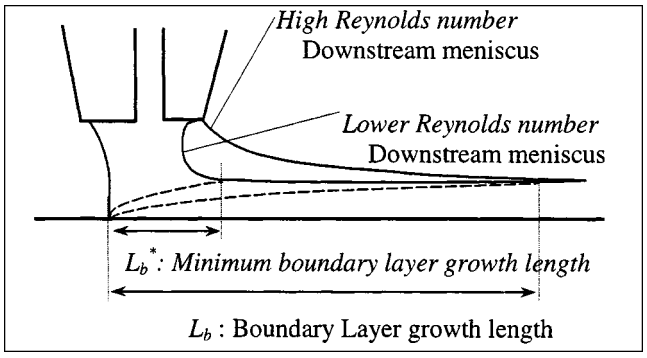

Figure 17. Boundary layer mechanism responsible for the high-inertia, low-flow limit.

speed below which the bead breaks. Equation 14 can be rearranged to give an approximate stability criterion at the high inertia regime:

$$\left[\frac{k\rho H_0}{\mu L_b^*}\right]^{1/2}\sqrt{V} > \frac{H_0}{t}. \qquad (15)$$

This square-root dependence of the critical gap-to-thickness ratio at the onset of the low-flow limit on web speed represents well the predicted critical conditions at the high inertia/Capillary low-flow limit, as illustrated in Figure 12. This simple boundary-layer argument can also explain the dependence of the critical condition on vacuum pressure. The length of the coating bead, and therefore the critical growth length L_b^*, increases as more and more vacuum is pulled in the upstream meniscus, leading to a smaller gap-to-film-thickness ratio.

Experimental Analysis

In order to validate the theoretical predictions presented in the previous section, experiments were conducted to obtain the critical ratio of gap to film thickness, above which the coating bead could not be sustained. In order to investigate the extended coating window predicted by the Navier-Stokes equations, the experiments were performed in a Capillary number range from 0.1 to 3.

Experimental procedure

The experimental setup is sketched in Figure 18. The coating liquid, composed of solid particles dissolved in an organic solvent (M.E.K.), was fed to the coating die using a gear pump. The flow rate was controlled by the pump speed. The die was 4 in. (10.16 cm) wide and had a slot height of 7 mil (177.8 μm). A polyester film was used as the substrate. The web speed varied from $V = 30$ ft/min up to $V = 350$ ft/min. Most of the deposited solvent evaporated before winding the substrate into a roll, leaving a solid coating over the substrate. However, at high speeds, some of the solvent was still present on the web. A scraper blade was used to remove the remaining solvent. In order to cover a wide range of Capillary numbers, solutions with different viscosity were used. The viscosity of the coating liquid was easily controlled by changing the concentration of solid particles on the solution. The viscosity range explored in this work extended from $\mu = 13$ cP to $\mu = 75$ cP. The liquid properties were measured with a shear rheometer and a cone and plate configuration. The viscosity was virtually independent of shear rate and there was no measurable normal stress difference, that is, the liquids were Newtonian in the range of shear rate where measurements were possible. The surface tension of the liquid was $\sigma = 25$ dyn/cm. The gap between the coating die and the substrate was fixed during the experiments at $H_0 = 4$ mil (101.6 μm), that is, the dimensionless slot height in the experiments was equal to the one used in the theoretical calculations.

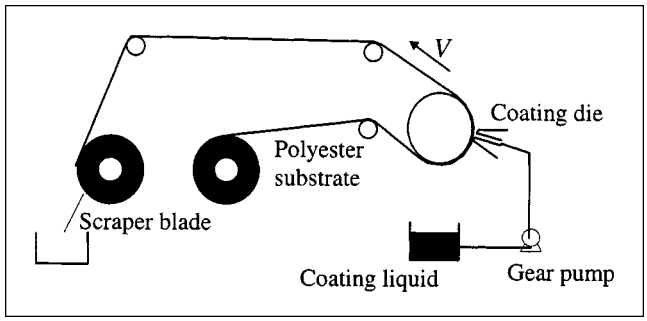

Figure 18. Experimental setup.

The critical gap-to-film thickness ratio at different line speeds was obtained using the following procedure:

1. The pump speed was set such that the thickness of the coated film was large, typically $H_0/t \approx 3$. A vacuum pressure was applied at the upstream free surface in order to establish the bead.

2. At constant web speed and vacuum, the rotation of the pump was decreased in small steps, until a uniform and continuous coating could not be formed. Typically one or two small stripes of uncoated substrate would appear. This point was considered to be the onset of the low-flow limit. The minimum film thickness was calculated from the flow rate and web speed. If the flow rate was diminished even more, alternating stripes of coated and uncoated substrate would form across the entire width of the wb, a coating defect known as a rivulet.

Results

The results of the experiments are summarized in Figure 19, which shows the critical gap-to-thickness ratio at different Capillary numbers obtained with four different coating solutions.

The scatter of the data can be attributed to the fact that the stability of the coating bead depends on the intensity of the disturbance that it is subjected to, and that these disturbances were not well controlled during the experiments. It is very hard to control and quantify the fluctuations on the line speed, vacuum pressure, pump speed and the localized imperfections of the substrate, and eventual bubbles in the solution fed into the die.

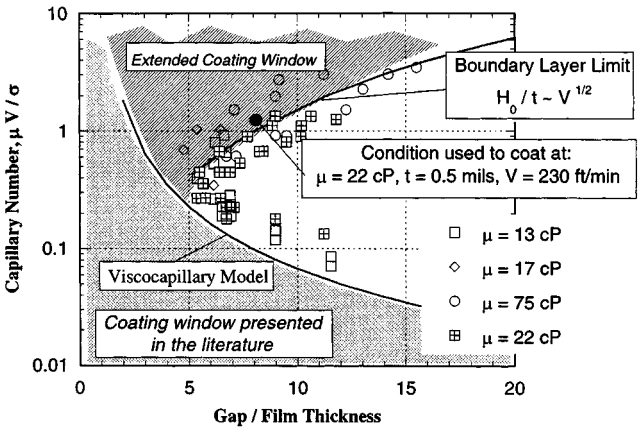

Figure 19. Measurements of critical gap-to-thickness ratio as a function of Capillary number.

The experimental results follow the same trend as the theoretical predictions. There are two distinct regimes. A low Capillary number regime, at which the minimum film thickness increases with line speed; and a high Capillary number regime, at which the minimum film thickness decreases with line speed. The data points obtained with the liquid of viscosity $\mu = 22$ cP extend from one regime to the other. The onset of the low-flow limit in the high inertia limit follows the square-root dependence on web speed as predicted by the boundary-layer theory; see Eq. 15.

The experiments indicate that the transition from the low Capillary number regime to the high Capillary number regime occurs at much smaller Property number P_p. With the coating gap used during the experiments, the Property number associated with the solution of viscosity $\mu = 22$ cP is $P_p = 5.2$. This value is two orders of magnitude smaller than the values used in the theoretical predictions ($P_p \approx 500$). A possible explanation for this discrepancy is that the coating die used in the experiments was much shorter than the one used in the theoretical analysis, leading to a much smaller critical boundary-layer growth length L_b^*.

Figure 19 also illustrates the coating window for slot coating predicted by the viscocapillary model and the extended region of stable coating at high Capillary number presented in this work. The single full circle on the graph represents an operating condition used to coat a liquid of viscosity $\mu = 22$ cP at a wet layer of thickness of $t = 0.5$ mil and line speed of $V = 230$ ft/min. These operating conditions are completely out of the coating window published in the literature, but inside the one reported here.

Final Remarks

Slot coating is one of the preferred methods for high precision coating. An important limitation of this method is when thin film are coated at relatively high speeds. This *low-flow* limit is caused by the receding action of the downstream free surface as the flow rate is reduced or the line speed raised. The operating parameters at which the coating bead breaks had been determined by previous researchers. However, the results were limited to low Capillary number flows.

In this work, the existence of a two-dimensional coating bead that leads to a continuous deposited liquid layer was studied by applying the film-profile equation (FPE) to describe the shape of the downstream free surface of the coating bead and also by solving the complete Navier-Stokes equations with free surfaces. This approach is not limited to low Capillary numbers and the Stokes approximation, that is, no inertial effects. The theoretical predictions were validated by experimental measurements.

At vanishing Reynolds number, the FPE model reproduces the Navier-Stokes predictions of the low-flow limit over the entire range of Capillary number explored. When inertia is negligible, even the simple viscocapillary model is very accurate at low Capillary number, as expected. The predicted low-flow limit is virtually the same for the three different models up to a Capillary number of 0.02. The relative difference between the viscocapillary model and the other two approaches is still below 10% up to Capillary number approximately equal to 0.1. When inertia is significant, a very interesting phenomenon is observed experimentally and predicted by the complete solution of the Navier-Stokes system: above a certain Capillary number, the minimum film thickness falls with increasing Capillary number, that is, thinner films can be obtained at faster web speeds. A detailed analysis of the flow indicates that, in the range of parameters explored, this behavior is apparently the effect of a viscous boundary layer. Formation of the boundary layer begins at the dynamic contact line, and grows over the length of the coating bead until it reaches the thickness of the liquid film. In this flow regime, the low-flow limit is affected by the length of the coating bead, which depends on the geometry of the coating device and the vacuum pressure applied. Neither the viscocapillary model nor the FPE include effects upstream of the downstream meniscus, and neither simulate this phenomenon.

The main conclusion of this work is that the operating parameter range at which slot coating can be used, that is, the coating window of the process, is larger than the one reported in the literature, broadening the applicability of this coating method.

Literature Cited

Beguin, A. E., "Method of Coating Strip Material," U.S. Patent No. 2,681,294 (1954).

de Santos, J. M., "Two-Phase Cocurrent Downflow Through Constricted Passages," PhD Thesis, Univ. of Minnesota, Minneapolis (1990).

Gates, I. D., "Stability Analysis of Slot Coating Flow," *AIChE Meeting*, New Orleans, LA (1996).

Higgins, B. G., and L. E. Scriven, "Capillary Pressure and Viscous Pressure Drop Set Bounds on Coating Bead Operability," *Chem. Eng. Sci.*, **35**, 673 (1980).

Keller, H. B., "Numerical Solution of Bifurcation and Nonlinear Eigenvalue Problems," *Applications of Bifurcation Theory*, P. H. Rabinowitz, ed., Academic Press, New York, (1977).

Kheshgi, H. S., "Profile Equations for Film Flows at Moderate Reynolds Number," *AIChE J.*, **35**, 1719 (1989).

Kheshgi, H. S., S. F. Kistler, and L. E. Scriven, "Rising and Falling Film Flow: Viewed from a First-Order Approximation," *Chem. Eng. Sci.*, **47**, 683 (1992).

Kistler, S. F., and L. E. Scriven, "Coating Flows," *Computational Analysis of Polymer Processing*, J. R. A. Pearson and S. M. Richardson, eds., Applied Science Publishers, London, p. 243 (1983).

Landau, L., and B. Levich, "Dragging of a Liquid by a Moving Plate," *Acta Physicochim.*, **17**, 42 (1942).

Lee, K. Y., and T. J. Liu, "Minimum Web Thickness in Extrusion Slot Coating," *Chem. Eng. Sci.*, **47**, 1703 (1992).

Ruschak, K. J., "Limiting Flow in a Pre-Metered Coating Device," *Chem. Eng. Sci.*, **31**, 1057 (1976).

Sartor, L., "Slot Coating: Fluid Mechanics and Die Design," PhD Thesis, Univ. of Minnesota, Minneapolis (1990).

Manuscript received June 10, 1999, and revision received Mar. 21, 2000.